Building and Environment 207 (2022) 108477

Contents lists available at ScienceDirect

Building and Environment

journal homepage: www.elsevier.com/locate/buildenv

Performance of fast fluid dynamics with a semi-Lagrangian scheme and an implicit upwind scheme in simulating indoor/outdoor airflow

Wei Liu [a,*], Haowen Sun [b], Dayi Lai [c], Yu Xue [b], Alan Kabanshi [d], Simon Hu [e]

[a] Department of Civil and Architectural Engineering, KTH Royal Institute of Technology, Brinellvägen 23, Stockholm, 100 44, Sweden
[b] School of Civil Engineering, Dalian University of Technology, Dalian 116024, China
[c] Department of Architecture, School of Design, Shanghai Jiao Tong University, Shanghai 200240, China
[d] Department of Building Engineering, Energy Systems and Sustainability Science, University of Gävle, 80176 Gävle, Sweden
[e] School of Civil Engineering, ZJU-UIUC Institute, Zhejiang University, Haining, 314400, China

ARTICLE INFO

Keywords:
Pressure-correction scheme
Numerical diffusion
Time step size
OpenFOAM

ABSTRACT

Computational fluid dynamics can be time consuming for predicting indoor airflows and pollutant transport in large-scale problems or emergency management. Fast fluid dynamics (FFD) is able to accomplish efficient and accurate simulation of indoor/outdoor airflow. FFD solves the advection term of the Navier–Stokes equations either by a semi-Lagrangian (SL) scheme or an implicit upwind (IU) scheme. The SL scheme can be highly efficient, but its first-order version is not conservative and introduces significant numerical diffusion. To improve its accuracy, a high-order temporal and interpolation scheme that not only reduces dissipation and dispersion errors but also guarantees the convergence speed should be applied. Otherwise, an IU scheme instead could be used to solve the advection term. The IU scheme is conservative and introduces minor numerical diffusion, but it may increase the computation time. Therefore, this study investigated the performance of FFD with SL scheme using high-order temporal and interpolation schemes and that with IU scheme. The comparisons used experimental data of two indoor airflows and one outdoor airflow. The results showed that FFD with IU scheme was overall more accurate than FFD with SL scheme. In simulating indoor airflow, both methods were robust and the predictions were independent of time step sizes if the Courant number was less than or equal to one. In simulating the outdoor airflow, the FFD with SL scheme performed better than the FFD with IU scheme for large time step sizes. The FFD with IU scheme consumed 44%–61% computing time of the FFD with SL scheme.

1. Introduction

The computational fluid dynamics (CFD) has been introduced to the indoor environment community for the prediction of air distribution since 1970s [1]. CFD numerically solves a set of partial differential equations, e.g. the Navier–Stokes equations, that governs the airflow and heat and species transport. With a validated turbulence model, CFD was able provide accurate and informative indoor air distribution with much less cost than the experimental measurements [2]. Therefore, CFD has been widely used as a research tool. Besides, CFD itself has also been investigated for improving its performance [3–5]. The performance of CFD is mainly dependent on its accuracy and efficiency. The accuracy of CFD could be enhanced by developing sophisticated turbulence models and near-wall treatment [6], generating mesh with sufficiently fine resolution [7], and implementing robust numerical algorithm and high-order numerical schemes [8], etc. In contrast, achieving efficient CFD simulation goes the opposite way, such as developing simplified turbulence models [9] and applying coarse mesh [10], etc. In engineering applications, it is critical to find the trade-off between the accuracy and efficiency.

The importance of efficient CFD simulations could be addressed in many engineering applications, such as indoor ventilation design [11], management of fire or accidental release of chemical/biological agents [12], real-time control of the heating, ventilation, and air-conditioning (HVAC) system [13], and large-scale problems like urban wind modeling [14], etc. The efficiency of CFD has been improved with increased computer powers during the past few decades. Besides, in the indoor environment community, researchers placed significant efforts on improving the computational speed in terms of parallel computing [15], reduced-order models such as recurrence CFD [16,17], and developing new numerical algorithms [18]. Fast fluid dynamics (FFD), which solves the Navier–Stokes equations by a non-incremental pressure-correction scheme [19] with a semi-Lagrangian (SL) scheme [20]

* Corresponding author.
E-mail address: weiliu2@kth.se (W. Liu).

https://doi.org/10.1016/j.buildenv.2021.108477
Received 25 August 2021; Received in revised form 6 October 2021; Accepted 18 October 2021
Available online 6 November 2021

Nomenclature

$\mathbf{U}$	velocity vector
p	air pressure
ρ	air density
$\mathbf{F}$	body forces
ν_{eff}	effective viscosity
t	flow time
$\mathbf{U}^n$	air velocity at previous time step
$\mathbf{U}^{n+1}$	air velocity at current time step
$\mathbf{U}^*$, $\mathbf{U}^{**}$	intermediate air velocities
p^{n+1}	air pressure at current time step
$\mathbf{X_a}$	arrival point
$\mathbf{X_d}$	departure point
$\mathbf{a}$	acceleration vector
i, j	cell index
TI	turbulence intensity
τ	computing time
ϕ	face volumetric flux
V	cell volume
Φ	normalized air quantity

specifically for the advection term, is able to provide detailed indoor airflow information as CFD does, but with improved efficiency.

FFD was originally developed by Stam [21] for computer games and then was introduced to indoor airflow simulation by Zuo and Chen [18]. The SL scheme solves the advection term by tracing the flow particle trajectory at each cell back in time to its former position and copies the quantities at that position to the present cell. The former position of a fluid particle may not be at the cell center, then an interpolation is needed to calculate the corresponding quantities. Since a linear interpolation scheme would cause conservation problems and introduce unwanted numerical diffusion [18], a hybrid interpolation scheme [22] or high-order interpolation scheme [23] was developed. A third-order backward and forward scheme developed by Mortezazadeh and Wang [23] is able to reduce both dissipation and dispersion errors and achieve an overall accuracy of fourth-order with lower computing cost than a typical fourth-order scheme.

The major advantage of the SL scheme is its unconditional stability for large time steps, thus offering fast solution. However, using an implicit upwind (IU) scheme instead of the SL scheme for the advection term would highly reduce the numerical diffusion and maintain the stability for large time steps [11]. Then one would question the necessity of using the SL scheme. Therefore, this study implements a non-incremental pressure-correction scheme with SL scheme using third-order backward and forward method (FFD with SL scheme) and that with an IU scheme (FFD with IU scheme) in OpenFOAM. This investigation compares the performance of these two solvers in terms of accuracy and efficiency in predicting two typical indoor airflows and outdoor wind. The impact of the time step size was also studied.

2. Methodologies

In this section, this study briefly describes the FFD with SL scheme and FFD with IU scheme in solving the Navier–Stokes equations for incompressible and viscous indoor/outdoor airflow:

$$\nabla \cdot \mathbf{U} = 0 \tag{1}$$

$$\frac{\partial \mathbf{U}}{\partial t} + (\mathbf{U} \cdot \nabla)\mathbf{U} = -\frac{1}{\rho}\nabla p + \nu_{eff}\nabla^2\mathbf{U} + \frac{1}{\rho}\mathbf{F} \tag{2}$$

where $\mathbf{U}$ is the velocity vector ; p the pressure, ρ the density; $\mathbf{F}$ the body forces; ν_{eff} the effective viscosity. The implementation of the two models in OpenFOAM is also introduced.

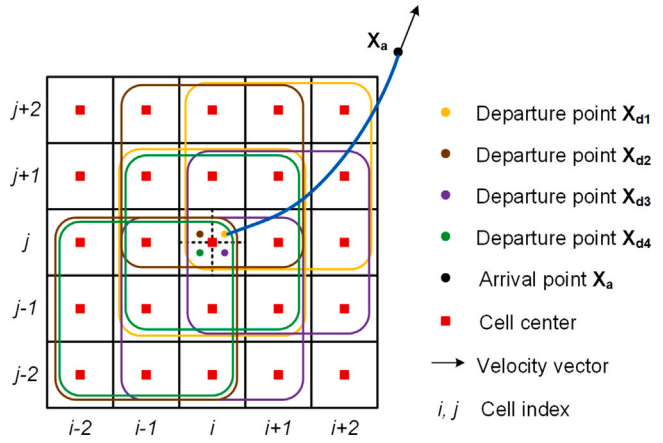

Fig. 1. Trace back and interpolation.

2.1. Fast fluid dynamics with semi-Lagrangian scheme

FFD with SL scheme applies a three-step time-advancement scheme that splits the momentum equation (Eq. (2)) into three discretized equations. By adopting the Euler backward implicit scheme for the temporary term, the three discretized equations are:

$$\frac{\mathbf{U}^* - \mathbf{U}^n}{\Delta t} = -(\mathbf{U}^n \cdot \nabla)\mathbf{U}^* \tag{3}$$

$$\frac{\mathbf{U}^{**} - \mathbf{U}^*}{\Delta t} = \nu_{eff}\nabla^2\mathbf{U}^{**} + \frac{1}{\rho}\mathbf{F}^n \tag{4}$$

$$\frac{\mathbf{U}^{n+1} - \mathbf{U}^{**}}{\Delta t} = -\frac{1}{\rho}\nabla p^{n+1} \tag{5}$$

where $\mathbf{U}^n$ and $\mathbf{U}^{n+1}$ represent the air velocity at the previous and current time steps, respectively; $\mathbf{U}^*$ and $\mathbf{U}^{**}$ are the intermediate air velocities; p^{n+1} represents the air pressure at the current time step. FFD solves Eqs. (3), (4), and (5) in sequence.

Eq. (3) could be solved by the SL scheme. As Fig. 1 shows, SL scheme traces the fluid particles at a cell center $\mathbf{X_a}$, which is called arrival point, back in time to the location $\mathbf{X_d}$, which is called departure point. The SL scheme then copies the flow properties at departure point $\mathbf{X_d}$ to arrival point $\mathbf{X_a}$. The departure point is determined by a second-order temporal scheme developed by Mortezazadeh and Wang [24], which considers both the air velocity and acceleration:

$$\mathbf{X_d} = \mathbf{X_a} - \frac{\Delta t^2}{2}\mathbf{a} - \Delta t\mathbf{U^n} \tag{6}$$

where $\mathbf{a}$ is the acceleration vector determined by:

$$\mathbf{a} = \frac{\mathbf{U^n} - \mathbf{U^{n-1}}}{\Delta t} \tag{7}$$

The location of the departure point may not be the center of a grid cell, then an interpolation is needed to obtain accurate estimation of the flow properties.

Since a linear interpolation would introduce significant numerical diffusion [22], this study adopted a backward 3rd-order interpolation at a one-time step and then a forward 3rd-order interpolation at the next time step alternatively [23]. The 3rd-order backward and forward interpolation needs the values in the surrounding nine cells (two-dimensional case), respectively. By naming the cell for departure point by departure cell, the nines cells to be used for interpolation are determined by the relative position between the departure point and departure cell center. For example, if the departure points is located at the upper right region of the departure cell (yellow dot $\mathbf{X_{d1}}$ in Fig. 2), the nine cells with departure cell as the central cell are for backward interpolation and the nine cells with departure cell as the lower left cell are for forward interpolation. Those cells are circled by yellow lines in

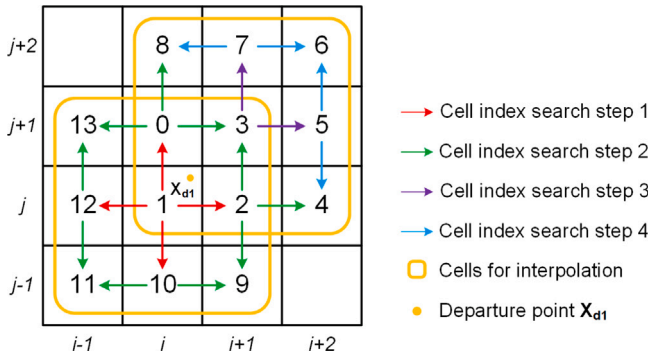

Fig. 2. Local cell index searching. (For interpretation of the references to color in this figure legend, the reader is referred to the web version of this article.)

Fig. 2. Therefore, the first step for interpolation is identifying the index of the departure cell.

This study adopted a local searching algorithm developed in OpenFOAM by Liu et al. [25] to identify the index for departure cell. Once the departure cell is identified, this study developed a four-step local cell index searching algorithm as shown in Fig. 2 for determining the others cells needed for interpolation. The step 1 finds the cells neighboring the departure cell. The step 2 finds all the cells for backward interpolation. Further, steps 3 and 4 identify all the cells for forward interpolation. The searching algorithm was extended to three-dimensional scenario. One can refer to [23] for the equations used to interpolate.

After the implementation of SL scheme for Eq. (3), Eq. (4) was solved iteratively by discretizing the Laplacian term by a Gauss linear orthogonal scheme, which specified linear interpolation scheme for the diffusion coefficient and the orthogonal treatment for surface normal gradient. Eq. (5) could not be solved directly as there were two unknown terms. [26] developed a pressure projection method that substituted Eq. (5) into the continuity equation Eq. (1), producing:

$$\frac{1}{\Delta t}\nabla\cdot\mathbf{U}^{**}=\frac{1}{\rho}\nabla^2 p^{n+1} \tag{8}$$

FFD again solved Eq. (8) iteratively by adopting a Gauss linear orthogonal scheme for pressure p^{n+1}. The pressure p^{n+1} was finally used to correct the air velocity by re-writing Eq. (5) as:

$$\mathbf{U}^{n+1}=\mathbf{U}^{**}-\frac{\Delta t}{\rho}\nabla p^{n+1} \tag{9}$$

In summary, the FFD with SL scheme requires cell index searching and interpolation. This study only considers the backward and forward interpolation for structured mesh, the developed solver is thus only applicable for structured mesh. This is also the reason for the orthogonal treatment for surface normal gradient in discretization.

2.2. Fast fluid dynamics with implicit upwind scheme

FFD with IU scheme in this study is a standard incremental pressure-correction scheme [19]. It applies a two-step time-advancement scheme that splits the momentum equation (Eq. (2)) into two discretized equations:

$$\frac{\mathbf{U}^{*}-\mathbf{U}^{n}}{\Delta t}=-(\mathbf{U}^{n}\cdot\nabla)\mathbf{U}^{*}+\nu_{eff}\nabla^2\mathbf{U}^{*}+\frac{1}{\rho}\mathbf{F}^{n}-\frac{1}{\rho}\nabla p^{n} \tag{10}$$

$$\frac{\mathbf{U}^{n+1}-\mathbf{U}^{*}}{\Delta t}=-\frac{1}{\rho}\nabla(p^{n+1}-p^{n}) \tag{11}$$

As Eq. (10) shows, the advection term and pressure is included implicitly and explicitly, respectively. A second-order upwind scheme was used to discretize the advection term. Eq. (11) is for the pressure difference and solved by the pressure projection method [26], which produces:

$$\frac{1}{\Delta t}\nabla\cdot\mathbf{U}^{*}=\frac{1}{\rho}\nabla^2(p^{n+1}-p^{n}) \tag{12}$$

The solved pressure difference $p^{n+1}-p^{n+1}$ is used to correct the air velocity by re-writing Eq. (11) as:

$$\mathbf{U}^{n+1}=\mathbf{U}^{*}-\frac{\Delta t}{\rho}\nabla(p^{n+1}-p^{n}) \tag{13}$$

One can notice that the FFD with IU scheme does not involve any cell index searching and interpolation, it could be directly applied to both structured and unstructured mesh. Its implementation is more straight forward than that of the FFD with SL scheme.

2.3. Scalar transport equations

In general, the indoor/outdoor airflow is turbulent and involves heat transfer. Therefore, the developed FFD solvers solved an extra energy equation and two other equations for turbulence kinetic energy k and turbulence dissipation rate ε in RNG $k-\varepsilon$ turbulence model. The RNG $k-\varepsilon$ model has been validated that it is capable of giving accurate prediction of indoor airflow [4] and has better performance than the other Reynolds Averaged Navier–Stokes (RANS) models in predicting the outdoor wind [27]. When the heat transfer was considered, this study adopted the Boussinesq approximation [28] to simulate the buoyancy effect. Since the energy equation and turbulent equations are both scalar transport equations, this study solved them by an iterative scheme, which was the same with we normally do. The convection terms were discretized by a second-order upwind scheme and the diffusion term by a Gauss linear orthogonal scheme.

3. Results

In order to compare the accuracy, efficiency, and robustness of the FFD with SL scheme and FFD with IU scheme, this investigation applied the developed solvers to predict the air distribution in three cases with experimental data for evaluation. The first two cases are forced convective and mixed convective indoor airflow from literature. The third case is outdoor airflow around a bunch of small-scale building blocks in a wind tunnel.

3.1. Case 1: forced convective indoor airflow

Case 1 is forced convection flow in a room with the dimension 2.44 m × 2.44 m × 2.44 m [29]. As shown in Fig. 3(a), the air supply inlet is located on the top of left wall and its height is 0.03 m. The outlet is located at the bottom of the right wall and its height is 0.08 m. In the center of the room, a box with the dimension 1.22 m × 1.22 m × 1.22 m is used to simulate the furniture. The air enters the room from the inlet at a speed of 1.366 m/s and a temperature of 22 ° C. The experiment by Wang and Chen [29] measured the air velocity at ten locations. This study used the experimental data on six representative locations as shown in Figs. 3(b) and 3(c) for validation.

This study used a structured mesh with the resolution of 47 × 42 × 48 according to the grid independence test by Wang and Chen [29]. For each numerical method, this investigation ran the simulation for 200 s physical flow time to obtain a steady-state airflow. In order to test the robustness of each model, each simulation begun with the most ambiguous time step size $\Delta t = 0.5$ s, the corresponding mean Courant number (Co_{mean}) was greater than one as summarized in Table 1. The Courant number (Co) is defined as:

$$Co=\Delta t\frac{\sum_{faces}|\phi|}{2V} \tag{14}$$

where ϕ is the face volumetric flux and V is the cell volume. A simulation with $\Delta t \geq 1.0$ s would diverge. Then this study gradually decreased the time step sizes and tested $\Delta t = 0.2$ s and $\Delta t = 0.1$ s.

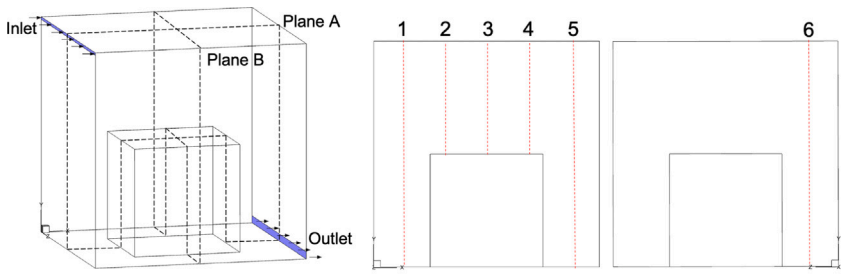

(a) Geometry (b) Plane A view (c) Plane B view

Fig. 3. Layout of a three-dimensional room [29].

Table 1
Mean Courant number for different time step sizes in case 1.

Δt (s)	0.1	0.2	0.5
FFD with SL	0.256	0.536	1.390
FFD with IU	0.324	0.645	1.395

Table 2
Mean Courant number for different time step sizes in case 2.

Δt (s)	0.1	0.2	0.5
FFD with SL	0.257	0.569	1.554
FFD with IU	0.324	0.645	1.395

Fig. 4 compares the predicted velocity profiles by FFD with SL scheme with the experimental data for case 1. The vertical axis was normalized by $H = 2.44$ m and the horizontal axis was normalized by the measured maximal air velocity $|\mathbf{U}|_{max} = 1.5$ m/s. The predictions with $\Delta t = 0.5$ s had minor difference from that by smaller time step sizes, which implied that the SL scheme with the high-order scheme for tracing back and interpolation would eliminate the numerical diffusion. The agreement between the predictions and the experimental data was well except that at position 5. Referring to the predicted airflow fields in Fig. 6(b), the FFD with SL scheme underestimated the jet development from the inlet. A possible reason is the assumption by SL scheme that the fluid properties follow the fluid particles in each time step. If a fluid particle originates out side the computational domain, the numerical scheme cannot yield an accurate result. Besides, the numerical estimation of the fluid particle trajectories bear absolutely no relationship to the physical ones.

The same comparisons for the FFD with IU scheme was provided in Fig. 5. Again, the predictions with $\Delta t = 0.5$ s had minor difference from that by smaller time step sizes. This was because the Co_{mean} was greater than one. Overall, the predictions by FFD with IU scheme had better agreement than that by the FFD with SL scheme with the experimental data. Especially at position 5, FFD with IU scheme had the correct prediction of the jet development, which was further confirmed by comparing the airflow fields in Fig. 6.

This study further compared the predicted air velocity by FFD and experimental data at monitored positions (72 sample points) in Fig. 7. The comparisons confirmed that the predictions by FFD with IU scheme were more accurate than that by the FFD with SL scheme. For large air velocities($|\mathbf{U}|/|\mathbf{U}|_{max} \geq 0.15$), both models were able to predict the air velocity with less than or equal to 10% error. It implied that both models were able to capture the major flow features. For small air velocities ($|\mathbf{U}|/|\mathbf{U}|_{max} < 0.15$), the FFD with IU scheme was able to predict the air velocity with less than or equal to 30% error at most positions. In contrast, the FFD with SL predicted the air velocity with greater than 30% error at most positions. It implied that the FFD with IU scheme was able to capture more flow details than the FFD with SL scheme. In terms of efficiency, the FFD with SL scheme required 50% more computing time than the FFD with IU scheme. This was because the implementation of the SL scheme took extra computing time in OpenFOAM [25].

3.2. Case 2: mixed convective indoor airflow

Based on case 1, case 2 added a 700 W heat source to the box in the room without changing the other setups [29]. The surface temperature of the box was 36.7 ° C that was higher than the air supply temperature of $T_{in} = 22.2$ °C. Then a thermal plume was introduced to investigate its impact on the flows. The numerical setup in this case was exactly the same with that of case 1. Table 2 summarized the tested time step sizes, mean Courant number, and computing time for 200 s physical flow time. The FFD with SL scheme required > 50% more computing time than the FFD with IU scheme.

Figs. 8 and 9 compares the predicted air velocity and temperature profiles by FFDs with experimental data at positions 2 (best agreement), position 3 (average agreement), and position 5 (worst agreement). The air velocity was normalized by the maximum velocity $|\mathbf{U}|_{max} = 1.5$ m/s found in the experiment. The air temperature was normalized by the maximum temperature $T_{max} = 36.7$ °C and minimum temperature $T_{min} = 22.2$ °C. The top and bottom figures in Figs. 8 and 9 were for the same position but with different properties. The predictions with $\Delta t = 0.2$ s and $\Delta t = 0.1$ s were almost the same and had minor difference from those with $\Delta t = 0.5$ s. The agreement between the FFD predictions and experimental data was the worst at position 5, which was consistent with observations by Wang and Chen [29]. The jet impacted on the wall at position 5 and the wall-bounded flow had strong curvature and separations. The recirculated airflow was further accelerated by the buoyancy force from the heated box. Both the FFD models were unable to fully handle such complex flows. However, the comparisons on the airflow fields on the stream-wise cross section in Fig. 10 clearly shows that the FFD with IU scheme better predicted the jet development and recirculated flow at position 5. The FFD with SL scheme under predicted the air temperature overall. It was attributed to the overall less accurate prediction of the airflow.

This investigation again compared the predicted air velocity and temperature by FFD and experimental data at the monitored positions (72 sample points) in Fig. 11. It is clear that the FFD with SL scheme was unable to predict the measured air velocity within 30% error at most positions. The FFD with SL scheme under predicted the measured air temperature overall. When $|\mathbf{U}|/|\mathbf{U}|_{max} \geq 0.15$, the FFD with IU scheme was able to predict the measured air velocities within 10% error. When $|\mathbf{U}|/|\mathbf{U}|_{max} \leq 0.15$, the FFD with IU scheme was able to predict the measured air velocities within 30% error at most positions. The FFD with IU scheme under predicted the measured air velocity at those points located at position 5. In terms of air temperature, the FFD with IU scheme was able to predict the measured air temperature within 10% error at most points. In summary, the FFD with IU scheme was more accurate than the FFD with SL scheme in predicting the mixed convection flow.

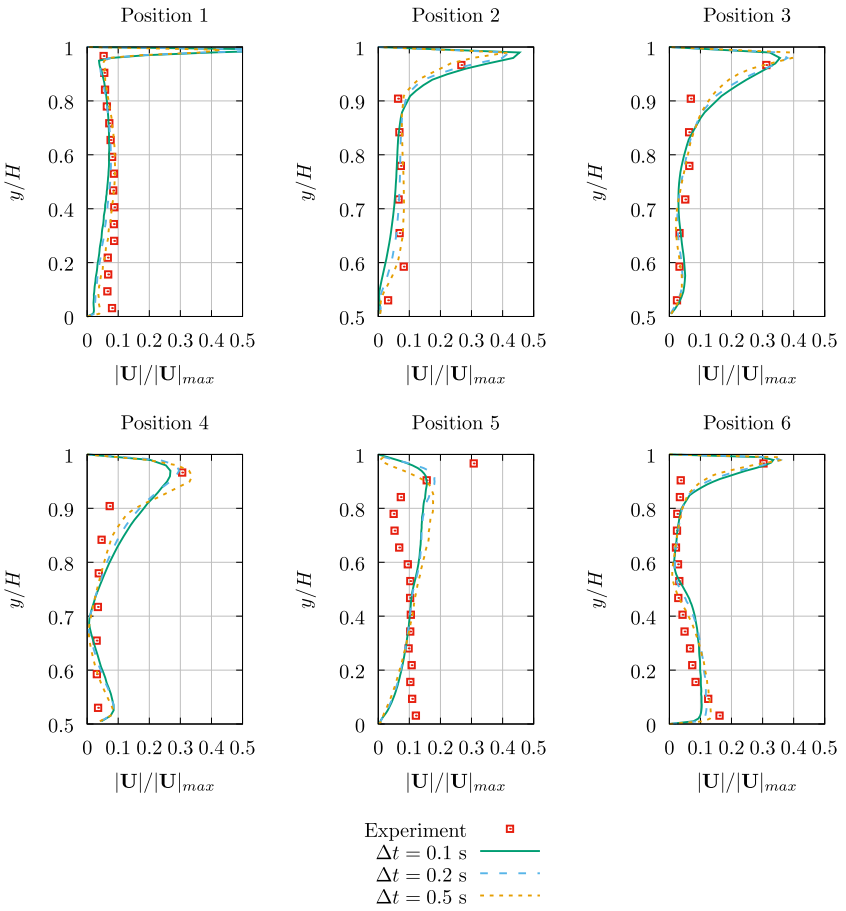

Fig. 4. Comparison of the predicted velocity profiles by FFD with SL scheme and experimental data for case 1.

3.3. Case 3: Outdoor airflow

The last case used for testing the FFD models was outdoor airflow simulated by an small-scale experiment in a wind tunnel [30]. The experiment placed 6 (rows) × 11 (columns) building blocks in a closed-circuit boundary layer wind tunnel designed for wind environmental assessment and ventilation studies. The size of each building block is $B \times B \times 2.67B$(height) with $B = 30$ mm. The building blocks were separated by streets with width B. The working section of the wind tunnel was 11 m long, 3 m wide and 1 .5 m high, which is much greater than the size of building arrays. Therefore, along the lateral direction, the computational domain only considered half of one column building blocks and half of the street as shown in Fig. 12. Further, Fig. 12(c) shows that two corresponding symmetrical boundary conditions were applied. Fig. 12(a) gives a side view of the computational domain. In accordance with the computational domain by Hang et al. [30], the inlet was $33.3B$ away from the first building block and the outlet was $121.3B$ away from the last building block. The height of the computational domain was $22.0B$. The experiment measured the upstream air velocity and turbulence intensity. For curve fitting the data points, this study adopted Eqs. (15) and (16) to implement the inlet boundary conditions. According to the grid independence study by Hang et al. [30], this study generated a mesh with near wall height $0.05B$, maximum size $0.25B$, and expansion ratio of 1.15. The near wall grid size was greater than that used by Hang et al. [30] because a wall function in OpenFOAM was adopted. The computational domain was discretized into 1.3 million hexahedra.

$$|\mathbf{U}_{in}|(z) = \begin{cases} 2.9(z/B)^{0.1616} & z < 6.7B \\ 3.91 & z \geq 6.7B \end{cases} \tag{15}$$

Table 3
Courant number for different time step sizes in case 3.

Δt (s)	FFD with SL	FFD with IU	Δt (s)	FFD with SL	FFD with IU
0.001	0.612	0.608	0.02	12.116	12.495
0.002	1.234	1.218	0.05	30.265	N/A
0.005	3.071	3.053	0.1	60.763	N/A
0.01	6.117	6.127			

$$TI(z) = \begin{cases} -0.0249(z/B) + 0.1327 & z < 5.28B \\ 0.00129 & z \geq 5.28B \end{cases} \tag{16}$$

Since the FFD with IU scheme showed overall better performance than the FFD with SL scheme in the first two cases, this study adopted the FFD with IU scheme for preliminary test by simulating the outdoor wind with time step size $\Delta t = 0.001$ s. The corresponding Co_{mean} was 0.608. The preliminary computation identified that a steady-state flow could be reached after five seconds physical flow. Therefore, the following computation simulate the airflow for five seconds. This study conducted the FFD simulations with multiple time step sizes as summarized in Table 3. The least time step size was $\Delta t = 0.001$ s that ensured the Co_{mean} was just less than one. The greatest time step size was $\Delta t = 0.1$ s and $\Delta t = 0.02$ s for FFD with SL and FFD with IU, respectively. This is because a prediction with even larger time step size differed significantly from the experimental data.

Figs. 13 and 14 compare the predicted air velocity with the experimental data at three typical locations V1, V6, and a line along the street centerline at $z = B$. The velocity was normalized by air velocity at the same height in the far upstream free flow $|\mathbf{U}|_{in}(z = B) = 2.9$ m/s. According to Fig. 12(c), V1 is located at the middle of the first two buildings and V6 is located 30 mm away from the last building. For the

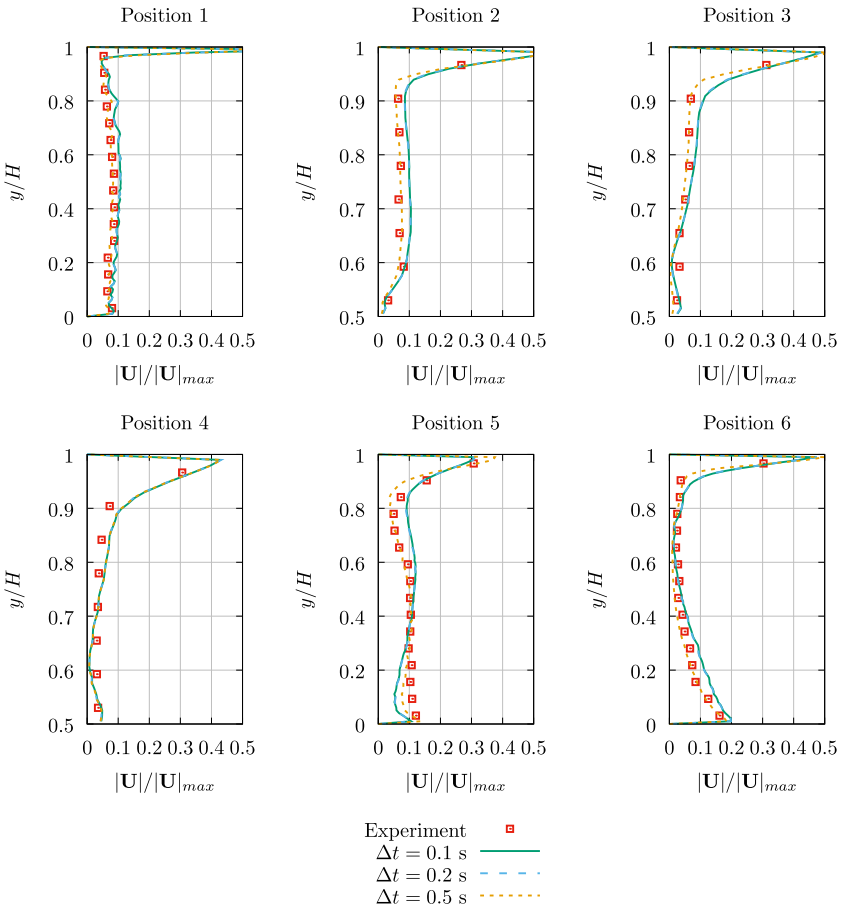

Fig. 5. Comparison of the predicted velocity profiles by FFD with IU scheme and experimental data for case 1.

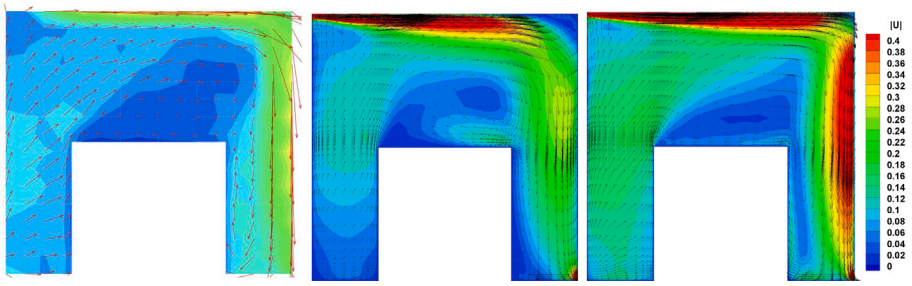

(a) Measured by Wang and Chen (2009) (b) FFD with SL (c) FFD with IU

Fig. 6. Measured [29] and predicted airflow on the stream-wise cross section for case 1.

FFD with SL scheme, it is clear that when $\Delta t \leq 0.002$ s or $\Delta t \geq 0.05$ s, the simulations either under predicted or over predicted the measured air velocity. When the $0.005 \text{ s} \leq \Delta t \leq 0.02$ s, the predictions agree well the experimental data. The FFD with SL was able to handle the simulation with large time step size. But the accuracy of the predictions were dependent on the time step size. The predictions by FFD with IU were independent of the time step sizes when $\Delta t \leq 0.005$ s and also agreed well with the experimental data. Please note that the Co_{mean} for $\Delta t = 0.005$ s is 3.053, which is greater than one. With $\Delta t \geq 0.01$ s, all the simulations over predicted the air velocity. Therefore, this study did not test the FFD with IU solver with $\Delta t > 0.02$ s. Overall, all the simulations under predicted the air velocity at those regions located behind the building blocks. This might be attributed to the inaccurate estimation of the flow separation in the downstream of the flow.

This study further plots the predicted airflow field with $\Delta t = 0.005$ s in the mid-cross section of the building ($y = B$) in Fig. 15. Both methods were able to predicted the recirculated airflow in the space between building blocks, which agreed well with the observations by Hang et al. [30]. However, the FFD with SL scheme was unable to predict the flow separation above the first building block. A possible reason would be weakness of SL scheme in simulating the convection of wall-bounded flow. The same weakness could also be observed in cases 1 and 2.

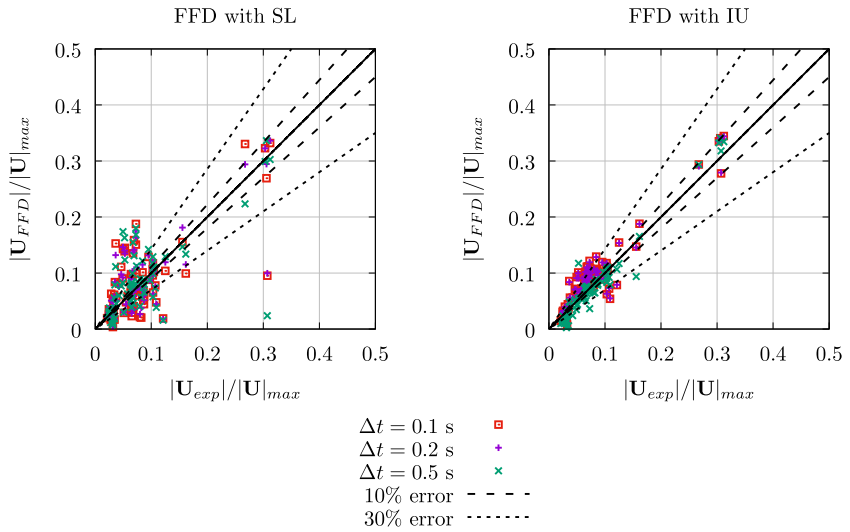

Fig. 7. Comparison of the predicted air velocity by FFD and experimental data at monitored positions for case 1.

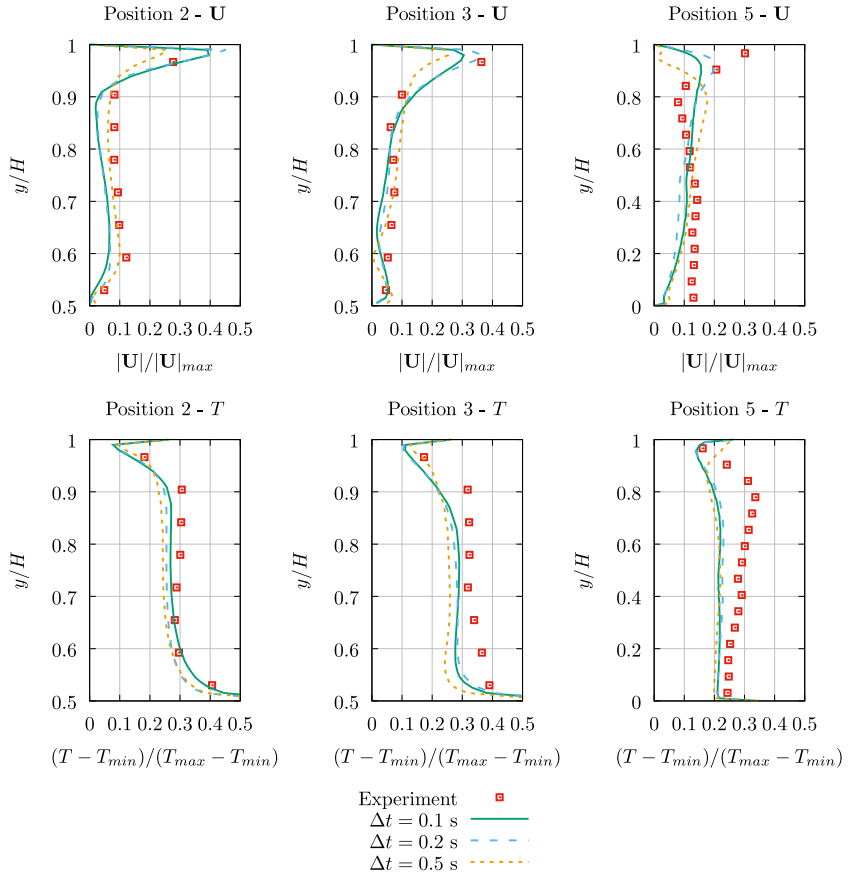

Fig. 8. Comparison of the predicted air velocity and temperature profiles by FFD with SL scheme and experimental data for case 2 at position 2: best agreement, position 3: average agreement, and position 5: worst agreement.

4. Discussions

4.1. Quantification of prediction accuracy

To quantitatively compare the overall accuracy of the FFD models, this study calculated the normalized root-mean-square deviation (NRMSD) between the experimental data and FFD predictions defined as:

$$NRMSD(\Phi) = \sqrt{\frac{\sum_{i=1}^{n}(\Phi_{exp,i} - \Phi_{numerical,i})^2}{n}} \quad (17)$$

where Φ is normalized air velocity or temperature. Table 4 provides the NRMSD for $\Delta t = 0.2$ s in cases 1 and 2 and $\Delta t = 0.005$ s in case 3. Those time step sizes ensure both FFD models give acceptable predictions. The results confirmed that FFD with IU scheme had better accuracy than

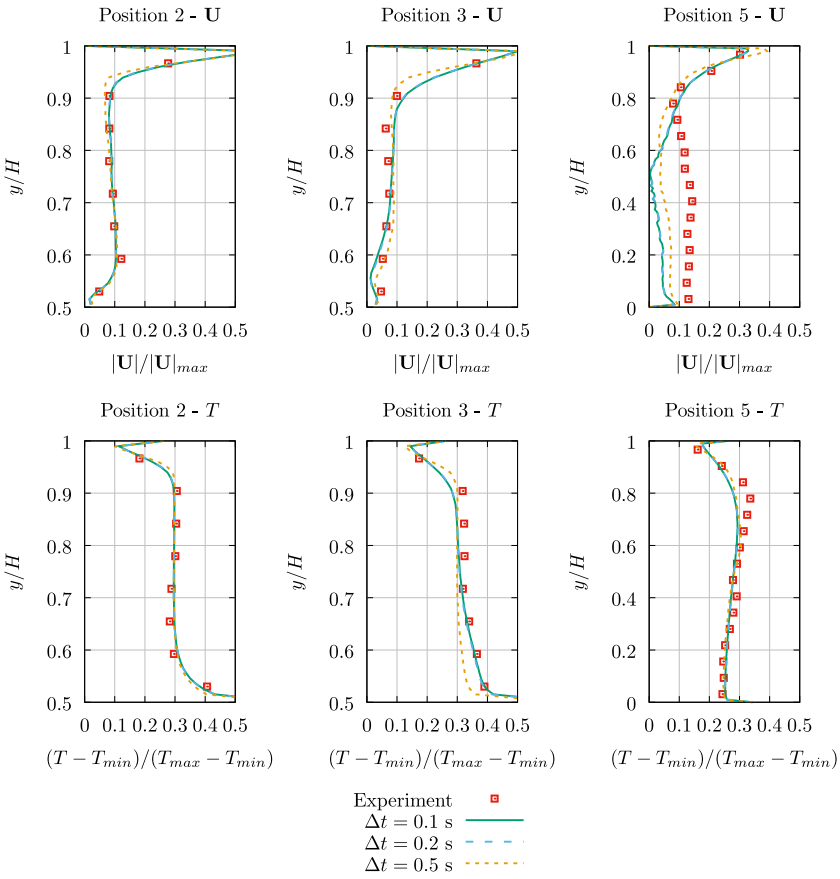

Fig. 9. Comparison of the predicted velocity and temperature profiles by FFD with IU scheme and experimental data for case 2 at position 2: best agreement, position 3: average agreement, and position 5: worst agreement.

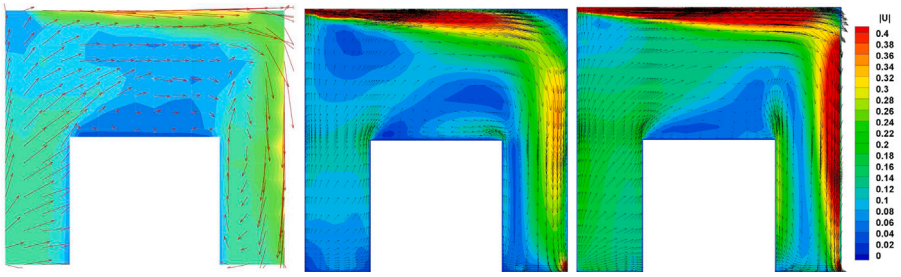

(a) Measured by Wang and Chen (2009) (b) FFD with SL (c) FFD with IU

Fig. 10. Measured [29] and predicted airflow on the stream-wise cross section for case 2.

FFD with SL scheme in predicting indoor airflow. For simulating the outdoor airflow, the FFD with SL scheme was slightly better.

4.2. Computing time

This investigation ran all the simulations with a Intel Xeon platinum 8179M processor with the frequency of 3.0 GHz and 96 Gb memories. Since the developed solver for FFD with SL scheme does not support parallel computing, this study ran all the simulations with just one core. Fig. 16 compares the computing time of FFD with SL scheme and FFD with IU scheme. The green cross represents the computing time for the tested scenarios. Their locations are determined by the computing time of FFD with SL scheme (horizontal axis) and the computing time of FFD with IU scheme (vertical axis). By using linear data fitting, the computing time with FFD with IU scheme was 61% and 44% of that with the FFD with SL scheme in cases 1 & 2 and case 3, respectively.

Table 4
Normalized root-mean-square deviation (NRMSD) between the experimental data and FFD predictions. (For cases 1 and 2, $|\mathbf{U}|^* = |\mathbf{U}|/|\mathbf{U}|_{max}$, where $|\mathbf{U}|_{max} = 1.5$ m/s and $T^* = (T - T_{min})/(T_{max} - T_{min})$, where $T_{min} = 22.2\,^\circ$C and $T_{max} = 36.7\,^\circ$C). For cases 3, $|\mathbf{U}|^* = |\mathbf{U}|/|\mathbf{U}|_{in}(z = B)$, where $|\mathbf{U}|_{in}(z = B) = 2.9$ m/s.

	Case 1	Case 2		Case 3
Δt (s)	0.2	0.2		0.005
Φ	$\lvert\mathbf{U}\rvert^*$	$\lvert\mathbf{U}\rvert^*$	T^*	$\lvert\mathbf{U}\rvert^*$
FFD with SL	4.7%	5.2%	7.0%	23.1%
FFD with IU	2.5%	4.2%	2.6%	24.6%

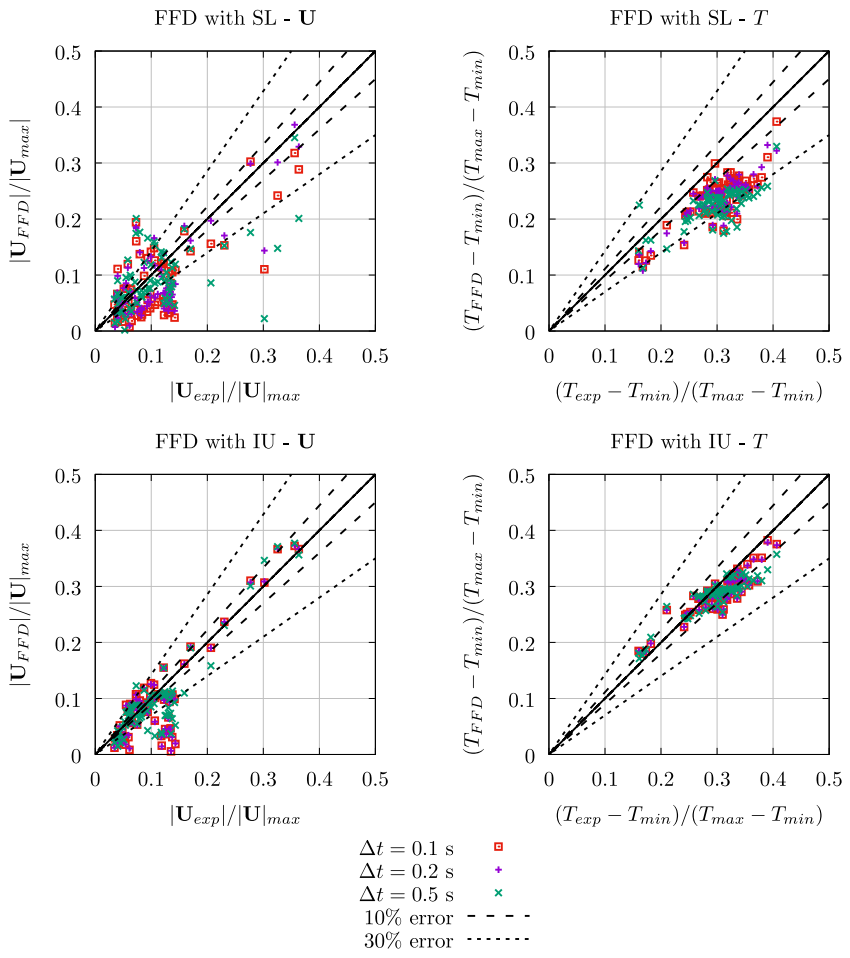

Fig. 11. Comparison of the predicted air velocity and temperature by FFD and experimental data at monitored positions for case 2.

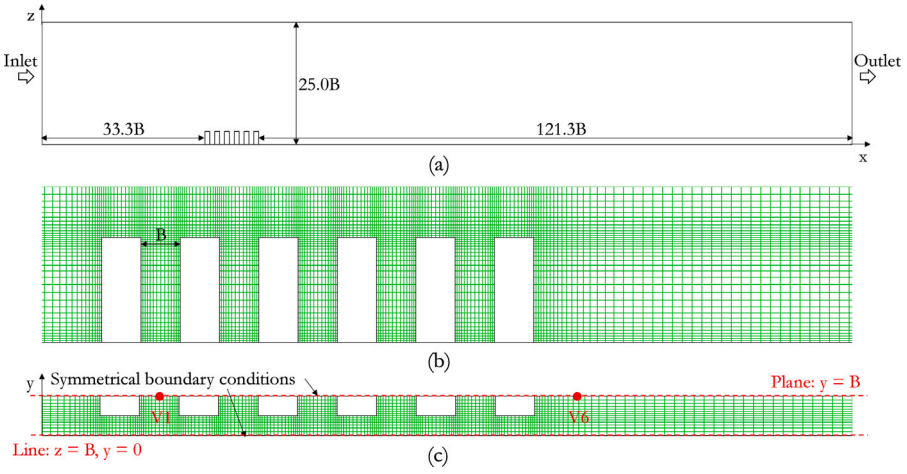

Fig. 12. (a) Computational domain, (b) side view of the mesh, and (c) top view of the mesh.

The current implementation of the SL scheme in OpenFOAM is less efficient than a second-order upwind scheme in solving the advection term. The implementation of the SL scheme could be accelerated if the mapping between the grid index and coordinates are known.

4.3. Limitations

A major limitation of the FFD with SL scheme is that the solver developed in OpenFOAM does not support parallel computing due to the SL scheme. The obstacle is that the departure point may locate in a decomposed zone other than that of the arrival point. Then the interpolation for the quantities at the departure point would be impossible or hard to handle. The FFD with IU scheme might be unable to give accurate prediction when the Co_{mean} is greater than one. This study only considered passive scalars, such as heat transfer. For non-passive scalars such as droplet or chemical reactions, extra source terms need to be added to the momentum equations. An implicit treatment of the corresponding source terms would not affect the stability of the

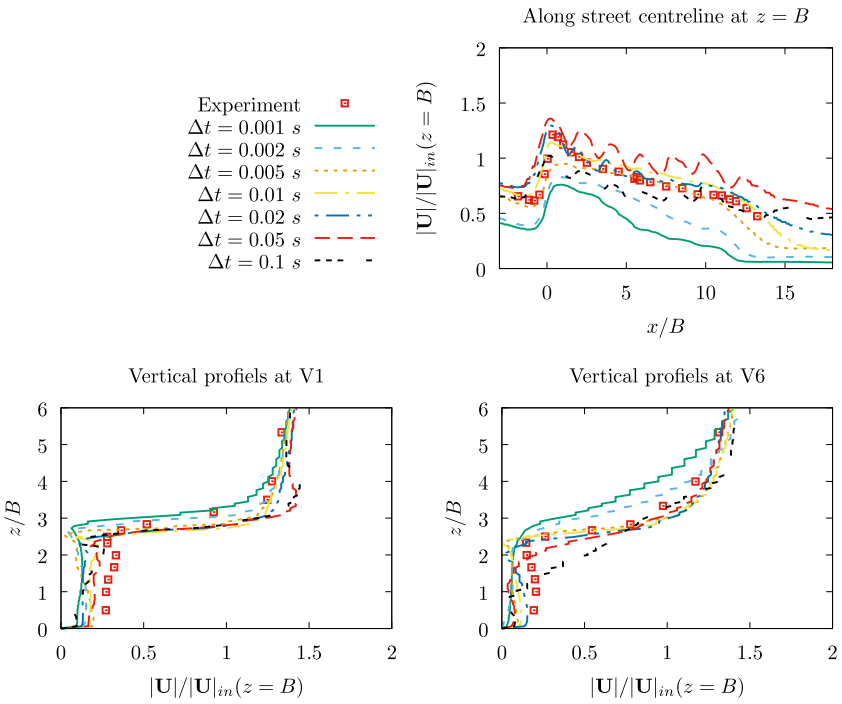

Fig. 13. Comparison between the predicted air velocity by FFD with SL scheme and experimental data for case 3.

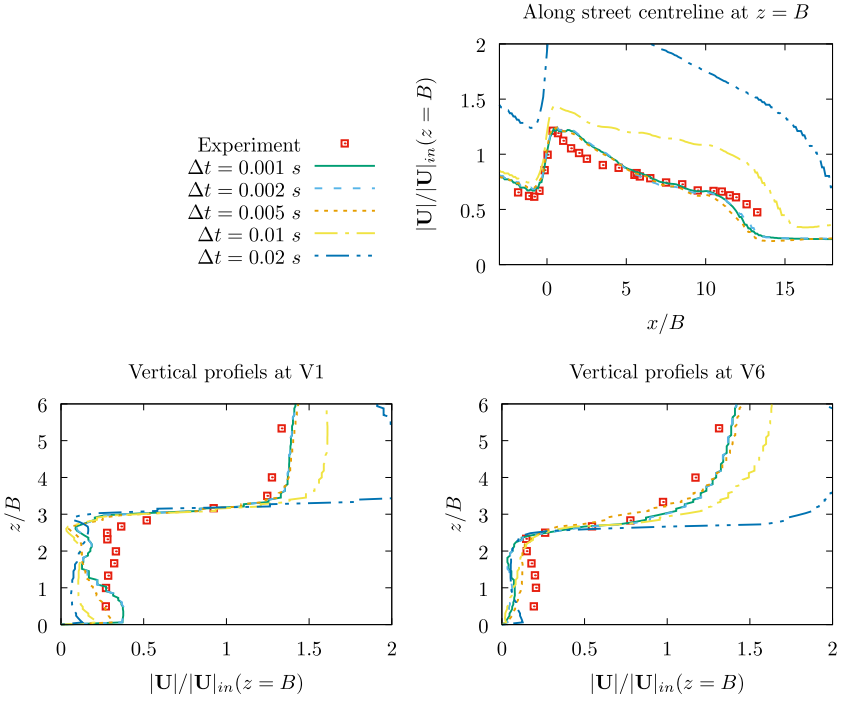

Fig. 14. Comparison between the predicted air velocity by FFD with IU scheme and experimental data for case 3.

discretized equations and the scheme should work. However, further validations are necessary.

5. Conclusions

This investigation compared the performance of FFD with SL scheme and FFD with IU scheme in predicting two typical indoor airflows and one outdoor airflow. The SL scheme used a second-order temporal scheme and a 3rd-order backward and forward interpolation, which were high-order temporal and spatial. The performance considered both the accuracy and efficiency that led to the following conclusions:

- For simulating the indoor airflow, the predictions by both methods were independent of time step size when the Co_{mean} was less than or equal to one. However, both methods were unable to handle the computation with large time step sizes. The predictions by FFD with SL were less accurate since the SL scheme might be inherently weak in predicting wall-bounded flow;

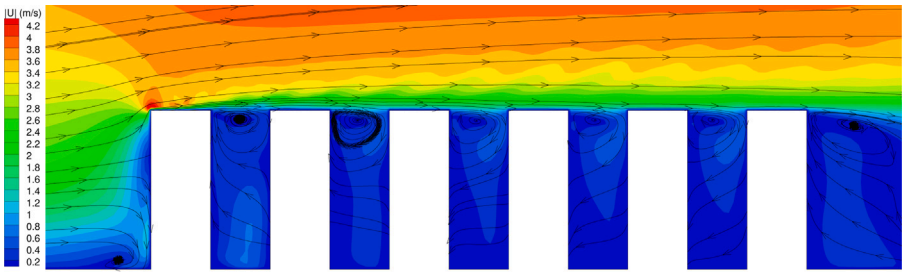

(a) FFD with SL

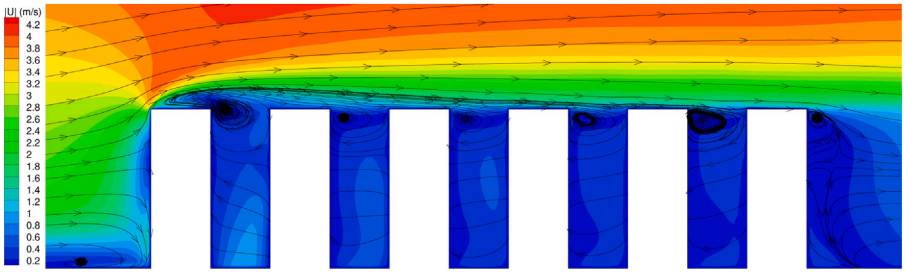

(b) FFD with IU

Fig. 15. Predicted flow fields in the cross section $y = B$.

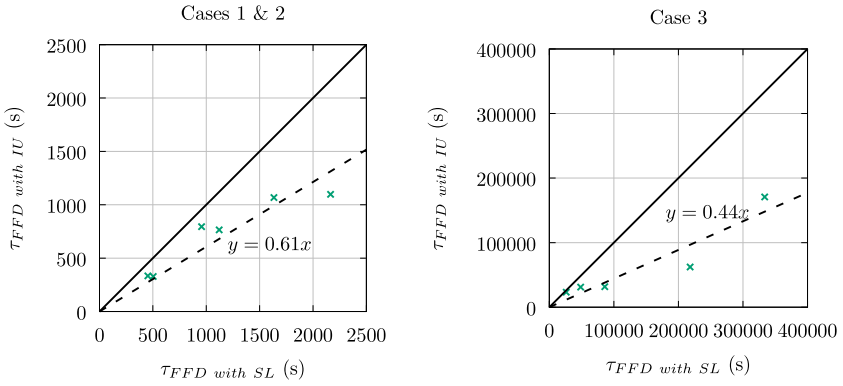

Fig. 16. Comparison of the computing time.

- For simulating the outdoor airlfow, the FFD with SL was able to give accurate prediction if an appropriate time step size was used. The appropriate time step size could corresponds to large mean Courant number. In contrast, the FFD with IU was unable to give accurate prediction if $\Delta t \geq 0.01$ s. When the Co_{mean} was less than or around one, the predictions by FFD with IU were independent of the time step size. In general, the FFD with SL was more capable than the FFD with SL in simulating outdoor airflow with large time step sizes;
- In the implementation of the numerical methods in OpenFOAM, the FFD with IU scheme consumed 44%–61% computing time of the FFD with SL scheme.

Declaration of competing interest

The authors declare that they have no known competing financial interests or personal relationships that could have appeared to influence the work reported in this paper.

Acknowledgment

This work was partially supported by the National Natural Science Foundation of China (Grant No. 51808487) and the Digital Futures, C3.ai DTI Research Award. This work was partially supported by the Zhejiang University/University of Illinois at Urbana-Champaign Institute, and was led by Principal Supervisor Simon Hu.

References

[1] P.V. Nielsen, Berechnung der luftbewegung in einem zwangsbelüfteten raum, Gesundheits-Ingenieur 94 (10) (1973).
[2] Q. Chen, Ventilation performance prediction for buildings: A method overview and recent applications, Build. Environ. 44 (4) (2009) 848–858.
[3] Z.J. Zhai, Z. Zhang, W. Zhang, Q.Y. Chen, Evaluation of various turbulence models in predicting airflow and turbulence in enclosed environments by CFD: Part 1—Summary of prevalent turbulence models, Hvac&R Res. 13 (6) (2007) 853–870.
[4] Z. Zhang, W. Zhang, Z.J. Zhai, Q.Y. Chen, Evaluation of various turbulence models in predicting airflow and turbulence in enclosed environments by CFD: Part 2—Comparison with experimental data from literature, Hvac&R Res. 13 (6) (2007) 871–886.

[5] P.V. Nielsen, Fifty years of CFD for room air distribution, Build. Environ. 91 (2015) 78–90.
[6] R. You, J. Chen, C.H. Lin, D. Wei, Q. Chen, Investigating the impact of gaspers on cabin air quality in commercial airliners with a hybrid turbulence model, Build. Environ. 111 (2017) 110–122.
[7] Z. Ai, C.M. Mak, Modeling of coupled urban wind flow and indoor air flow on a high-density near-wall mesh: Sensitivity analyses and case study for single-sided ventilation, Environ. Model. Softw. 60 (2014) 57–68.
[8] V. Vuorinen, J.-P. Keskinen, C. Duwig, B. Boersma, On the implementation of low-dissipative Runge–Kutta projection methods for time dependent flows using OpenFOAM®, Comput. & Fluids 93 (2014) 153–163.
[9] Q. Chen, W. Xu, A zero-equation turbulence model for indoor airflow simulation, Energy Build. 28 (2) (1998) 137–144.
[10] M. Jin, W. Liu, Q. Chen, Simulating buoyancy-driven airflow in buildings by coarse-grid fast fluid dynamics, Build. Environ. 85 (2015) 144–152.
[11] W. Liu, R. You, J. Zhang, Q. Chen, Development of a fast fluid dynamics-based adjoint method for the inverse design of indoor environments, J. Build. Perform. Simul. 10 (3) (2017) 326–343.
[12] L. Wang, Q. Chen, Applications of a coupled multizone-CFD model to calculate airflow and contaminant dispersion in built environments for emergency management, Hvac&R Res. 14 (6) (2008) 925–939.
[13] W. Tian, T.A. Sevilla, W. Zuo, M.D. Sohn, Coupling fast fluid dynamics and multizone airflow models in Modelica Buildings library to simulate the dynamics of HVAC systems, Build. Environ. 122 (2017) 269–286.
[14] B. Blocken, Computational fluid dynamics for urban physics: Importance, scales, possibilities, limitations and ten tips and tricks towards accurate and reliable simulations, Build. Environ. 91 (2015) 219–245.
[15] J. Cohen, M.J. Molemaker, A fast double precision CFD code using CUDA, Parallel Comput. Fluid Dyn. Recent Adv. Future Dir. (2009) 414–429.
[16] Y. Du, B. Blocken, S. Pirker, A novel approach to simulate pollutant dispersion in the built environment: Transport-based recurrence CFD, Build. Environ. 170 (2020) 106604.
[17] Y. Du, B. Blocken, S. Abbasi, S. Pirker, Efficient and high-resolution simulation of pollutant dispersion in complex urban environments by island-based recurrence CFD, Environ. Model. Softw. (2021) 105172.
[18] W. Zuo, Q. Chen, Real-time or faster-than-real-time simulation of airflow in buildings, Ind. Air 19 (1) (2009) 33.
[19] J.-L. Guermond, P. Minev, J. Shen, An overview of projection methods for incompressible flows, Comput. Methods Appl. Mech. Engrg. 195 (44–47) (2006) 6011–6045.
[20] R. Courant, E. Isaacson, M. Rees, On the solution of nonlinear hyperbolic differential equations by finite differences, Comm. Pure Appl. Math. 5 (3) (1952) 243–255.
[21] J. Stam, Stable fluids, in: Proceedings of the 26th Annual Conference on Computer Graphics and Interactive Techniques, 1999, pp. 121–128.
[22] W. Zuo, M. Jin, Q. Chen, Reduction of numerical diffusion in FFD model, Eng. Appl. Comput. Fluid Mech. 6 (2) (2012) 234–247.
[23] M. Mortezazadeh, L.L. Wang, A high-order backward forward sweep interpolating algorithm for semi-Lagrangian method, Internat. J. Numer. Methods Fluids 84 (10) (2017) 584–597.
[24] M. Mortezazadeh, L.L. Wang, Solving city and building microclimates by fast fluid dynamics with large timesteps and coarse meshes, Build. Environ. (2020) 106955.
[25] W. Liu, M. Jin, C. Chen, R. You, Q. Chen, Implementation of a fast fluid dynamics model in OpenFOAM for simulating indoor airflow, Numer. Heat Transfer A 69 (7) (2016) 748–762.
[26] A.J. Chorin, Numerical solution of the Navier-Stokes equations, Math. Comp. 22 (104) (1968) 745–762.
[27] A. Ricci, I. Kalkman, B. Blocken, M. Burlando, M. Repetto, Impact of turbulence models and roughness height in 3D steady RANS simulations of wind flow in an urban environment, Build. Environ. 171 (2020) 106617.
[28] J. Boussinesq, Analytical Theory of Heat Harmonized with Thermodynamics and with the Mechanical Theory of Light: Tome I- [II] ..., Vol. 2, Gauthier-Villars, 1903.
[29] M. Wang, Q. Chen, Assessment of various turbulence models for transitional flows in an enclosed environment (RP-1271), Hvac&R Res. 15 (6) (2009) 1099–1119.
[30] J. Hang, Y. Li, M. Sandberg, Experimental and numerical studies of flows through and within high-rise building arrays and their link to ventilation strategy, J. Wind Eng. Ind. Aerodyn. 99 (10) (2011) 1036–1055.